https://doi.org/10.5194/egusphere-2025-2214
Preprint. Discussion started: 11 July 2025

EXSoDOS 1.0: downscaling of weather extremes shifts for ensemble climate projections using ground-based measurements, reanalysis and stochastic modelling

Hendrik Wouters[1], Jente Broeckx[1], Francisco Pereira[1], Boucary Dara[2], Afoussatou Diarra[2], Robin Houdmeyers[1], and Dirk Lauwaet[1]

[1]Flemish Institute for Technological Research (VITO), Boeretang 200, B-2400, Mol, Belgium
[2]National Meteorological Agency of Mali (MALI-METEO), Route Aeroport Bamako Senou, Bp 237, Bamako, Mali

Correspondence: Hendrik Wouters (hendrik.wouters@vito.be)

Abstract. Accurately representing the changes of local extreme weather events in climate projections is crucial for climate impact assessment and adaptation services. Climate models often struggle with capturing these events due to their coarse spatial resolution. Existing downscale products successfully reduce overall biases of past or future climateological variables, but the representation of variability and extreme events including their past and future shifts under climate change are still not addressed. A new stochastic model, EXSoDOS, addresses this gap by the DOwnScaling of weather EXtremes Shifts for ensemble climate projections using ground-based measurements, reanalysis, and global climate models. This is done by using a stochastic model that correlates coarse-scale gridded historical climate records with the point-scale measurements. Therefore, EXSoDOS combines ground-based data (either from the Global Historical Climatological Network or user-specified), ERA5 reanalysis, and global climate model (GCM) projections to downscale past and future daily climate records. We demonstrate EXSoDOS for 5 use cases, resp. daily minimum temperature in Belgium, daily maximum temperature in Azerbaijan, heat stress in India, wind velocity in Germany and precipitation in Mali. It is found that EXSoDOS is able to represent annual cycle variability, density distributions, and extreme events of return periods of up to 10 years, while they are all underrepresented by the raw GCM outputs. Observed tendencies towards more extremes between two past periods 1961–1990 and 1991–2020 are also better represented. Projections under the SSP585 scenario suggest amplified extremes in maximum temperature, precipitation, and heat stress by 2071–2100. Furthermore, downscaling affects the outcomes of shifting extremes under future climate change, which is evident in terms of both absolute and relative changes, as well as changes in return periods. While limitations of statistical downscaling persist, it is concluded that EXSoDOS offers a novel method for estimating past and future shifts in weather extremes for weather stations with a sufficient daily record of data of multiple decades.

1 Introduction

Global (Eyring et al., 2016) and regional (Katragkou et al., 2024; Coppola et al., 2021) climate model initiatives have been succesful in predicting many aspects of climate change, like increasing temperature and shifts in precipitation amounts. However, events like heavy precipitation, heavy wind, extreme heat (stress) and cold spells are generally underrepresented in climate pro-

https://doi.org/10.5194/egusphere-2025-2214
Preprint. Discussion started: 11 July 2025

jections. This results from their coarse spatial resolution for which the scale of the extreme events are too small to be resolved. Particularly, meteorological point-scale observations generally show much more erratic temporal variability than the coarser-scale gridded products. Especially, extreme precipitation and wind, but also temperature and heat stress, can be influenced by confounding local climate effects resulting in local features like local convective precipitation events and urban heat islands. However, local extreme weather events have large impacts on society, infrastructure and ecosystems. Hence, their underrepresentation hampers extreme hazard assessment and their impacts under climate change. Not only the absolute representation but also the shifts of extreme weather distributions under past and future climate change are crucial for climate risk assessment and adaptation planning (int, 2023).

Several techniques have been developed to downscale global (Eyring et al., 2016) and regional (Katragkou et al., 2024; Coppola et al., 2021) climate projections to represent their small-scale climate effects. On the one hand, they include mechanistic downscaling using convection permitting atmospheric numerical models with a resolution of 7km down to 1km (Kendon et al., 2021), high enough to resolve deep convection and associated extreme precipitation (Vanden Broucke et al., 2019; Brisson et al., 2016) and local land use like urban areas (Wouters et al., 2016; De Ridder et al., 2015). they have been effective to project extreme weather events (Fosser et al., 2024; Termonia et al., 2018; Wouters et al., 2017; Saeed et al., 2017) on the other hand, statistical downscaling methods have been developed (Maraun, 2016) to finer resolution grids (Lange, 2019; Karger et al., 2023) and point observation locations (Switanek et al., 2022).

However, future climate assessment of local extremes is hampered by the requirements of computatational resources and input data requirements. Particularly, mechanistic downscaling with atmospheric numerical models are computationally very demanding since higher-resolution climate also requires smaller integration time step becacuse of the courant-frederich-levichs criterium (Prein et al., 2015). The most recent point-location stochastic downscaling models (Switanek et al., 2022; Volosciuk et al., 2017; Devis et al., 2013) and weather generators (Van De Velde et al., 2023; Brisson et al., 2015) have only applied to specific areas or variables, or have not been applied to future climate projections. Gridded downscaling products may either have a low resolution (Lange, 2019) or do not cover ensemble future climate either (Karger et al., 2023). While these different downscaling products can reduce overall biases of coarse-scale products, their representation of extremes in terms of variability, distributions and their return periods as observed from weather stations are not addressed, let stand the shifts under past and future climate change.

To fill this gap, we present EXSoDOS, a DOwnScaling method of weather EXtremes Shifts for climate projections using ground-based measurements, reanalysis, global climate models, and statistical downscaling. It downscales time series from an ensemble of global climate models to represent the variability and extremes as observed by weather stations. The model implements a stochastic downscaling technique that is calibrated on point-scale observations and coarse-scale reanalysis, with over 84 years of climate historical climate data (from 1940 to present). Hereby, historical coarse-scale reanalysis data and observations are normalized and correlated with each other. The method can be used at locations where climatological records of observations are available. It can either employ observational data from the Global Historical Climate Network (GHCN) hosted by the National Oceanic and Atmospheric Administration (NOAA; https://www.ncei.noaa.gov/products/land-based-station/global-historical-climatology-network-daily), or ingest data from local observational sources, eg., measurements carried out

https://doi.org/10.5194/egusphere-2025-2214
Preprint. Discussion started: 11 July 2025

by national meteorological offices, agro-meteorological or envionmental institutes. In the case of the latter, one only requires the position (in latitude longitude coordinates) and the observed time series in a commonly used format (csv or parquet). The stochastic model is then applied on multi-member climate projections towards 2100 after bias-correcting them with reanalysis data. As such, the method follows the downscaling strategy proposed by (Switanek et al., 2022), and is further designed to represent climate extremes regarding different weather variables including daily minimum and maximum temperature, heat stress temperature and wind speed. To evaluate the representation of extreme events with respect to observations and their shifts under past and future climate change, a number of statistics are employed, including the daily-to-annual variability, density distributions and overlaps, and return periods.

EXSoDOS runs quickly and automatically, and can be applied at locations where a sufficiently extensive record of observations from weather stations are available, preferably 30 years of continuous data record or longer. It is also easily applicable by requiring only a few parameters, particularly the station coordinates, the weather time series under scope (either temperature, precipitation, wind, or heat stress). The synthesis of time series for a handful of stations and a handful of climate model members and climate scenarios takes less than an hour on a contemporary desktop computer, resulting in a negligible carbon footprint of computer resources. Our service is demonstrated for several specific use cases across the globe, in which the statistical model is calibrated and validated on historical data, and applied on climate projections. The demonstration is featured by metrics common to extremes climate assessment, including annual cycles, density distributions and return periods.

The structure of the remaining of this paper is as follows. In the methods section 2, the program interface with global data sources, the downscaling procedure, and bias correction are described. The statistics for validation and assessment as well as the case areas are described after. In the results section 3, we perform a validation of the model output for the historical period, and the assessment with climate projections for each of the use cases. We conclude the paper with perspectives and challenges for extreme weather assessment under climate change in section 4.

2 Method

To perform the downscaling, coarse-scale predictors (x) are correlated to the point-scale predictands (y). Calibration and validation of the statistical model is done on the basis of historical reanalysis reconstruction x_r and the measurements from the weather stations y_o. While ensemble models of climate projections offer the statistical climate properties on the multi-annual time series including anomalies, they are not in synchrony with observations or, in other words, their sequence of weather patterns generally differ from that of the observations. Consequently, they cannot be used to correlate the coarse-scale model output with local measurements. Therefore, historical reanalysis, which is constrained and in synchrony with the observations, is used for the calibration. For calibration, half of the days in the time series are chosen randomly for calibration (x_r^c, y_o^c) and the other half for validation (x_r^v, y_o^v). Finally, the downscaling is applied on the climate model projections x.

To ensure scale consistency of the predictors between calibration phase and application phase, the climate reanalysis is upscaled to the climate model grid for each individual model. Furthermore, the downscaling procedure follows the perfect prognosis assumption (Maraun, 2016), which means that the predictor is describing the reality free from biases. Therefore,

https://doi.org/10.5194/egusphere-2025-2214
Preprint. Discussion started: 11 July 2025

the biased predictors from the climate models (x_b) are bias-adjusted with a quantile-delta mapping procedure (Cannon et al., 2015), see also section 2.3. The downscaling strategy above leads to the following subsequent steps, see also fig. 1:

1. Acquire climate reconstruction (reanalysis) and upscale to the climate model grid by aggregation and interpolation
2. Acquire historical predictand (y_o) from weather stations
3. Extract historical predictor (x_r) from upscaled reanalysis at point locations of the weather stations
4. Randomly select half of the historical data for model calibration (x_r^c and y_r^c) and the remaining half for model validation (x_r^c and y_r^c)
5. calibration of the statistical model using x^c and y^c (section 2.2)
6. Validation of the statistical model using x_r^v and comparing the output with y_r^v, see section 2.4)
7. Acquire (biased) climate projections for point locations (x_b)
8. Climate projections are bias-adjusted (indicated with x_m) with upscaled reanalysis using quantile-delta mapping, section 2.3)
9. Synthesis of downscaled climate projections (y_m) by applying the statistical model on bias-adjusted climate projections (section 2.5)

As such, the procedure performs bias-adjustment at the coarse scales and statistical downscaling towards the point scale in separate steps. This avoids inconsistencies arising from mixing up statistical properties (particularly, quantile values) across spatial scales. The latter could occur if one would apply the statistical downscaling directly on the climate model output without bias-adjustment on the grid level. Especially, trends under climate change including those of the (extreme) quantile values at the local scales can differ to those (spatially aggregated) at the coarse scales, so these should not be used for one another. As shown by (Maraun, 2013), mapping point-scale quantiles to coarse-scale quantiles, or vice versa, may lead to unrealistic trends of extremes leading to misinterpretation. The strategy of scale separation where scale transition is established with a statistical model only after bias-adjustment at the model grid level is in accordance to previous methods (Lange, 2019; Switanek et al., 2022; Volosciuk et al., 2017), and advised by previous analyses (Maraun, 2013).

The different processing steps are implemented in Python and computationally optimized as vectorized numerical operations with Python Xarray, Pandas and NumPy.

In the next subsections, we elaborate the input data sets, the statistical downscaling and bias-adjustment in more detail.

2.1 Input

Observations collected from GHCN are used as predictand for calibration and validation. It includes 10010 stations for which it reports an available record of at least 30-years, see Fig. 2. Alternatively, the service is able to read observational data provided

https://doi.org/10.5194/egusphere-2025-2214
Preprint. Discussion started: 11 July 2025

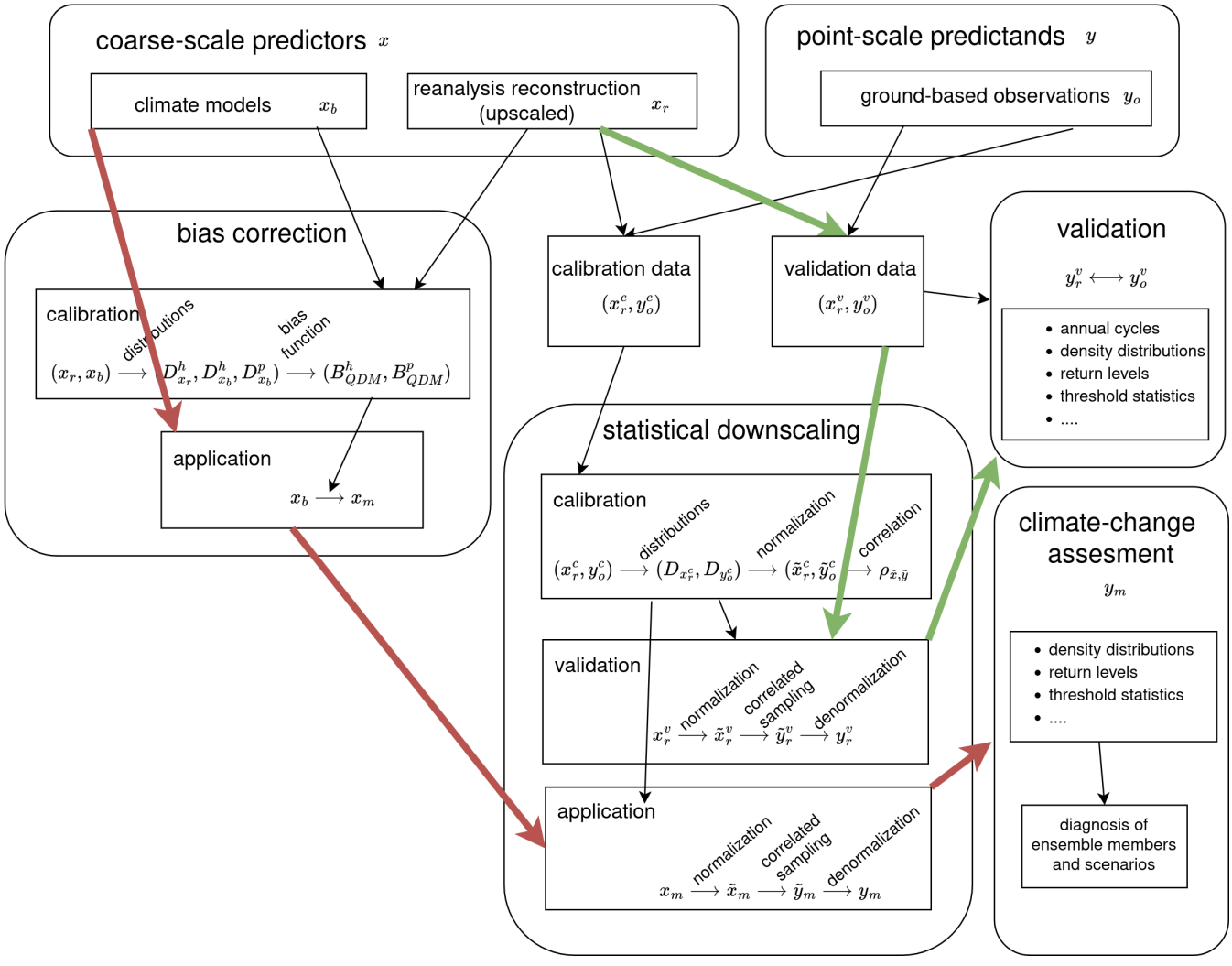

Figure 1. overview of EXSoDOS. The green arrows indicate the validation steps starting from the reanalysis reconstruction, whereas the red arrows indicate the assessment steps starting from the climate models.

https://doi.org/10.5194/egusphere-2025-2214
Preprint. Discussion started: 11 July 2025

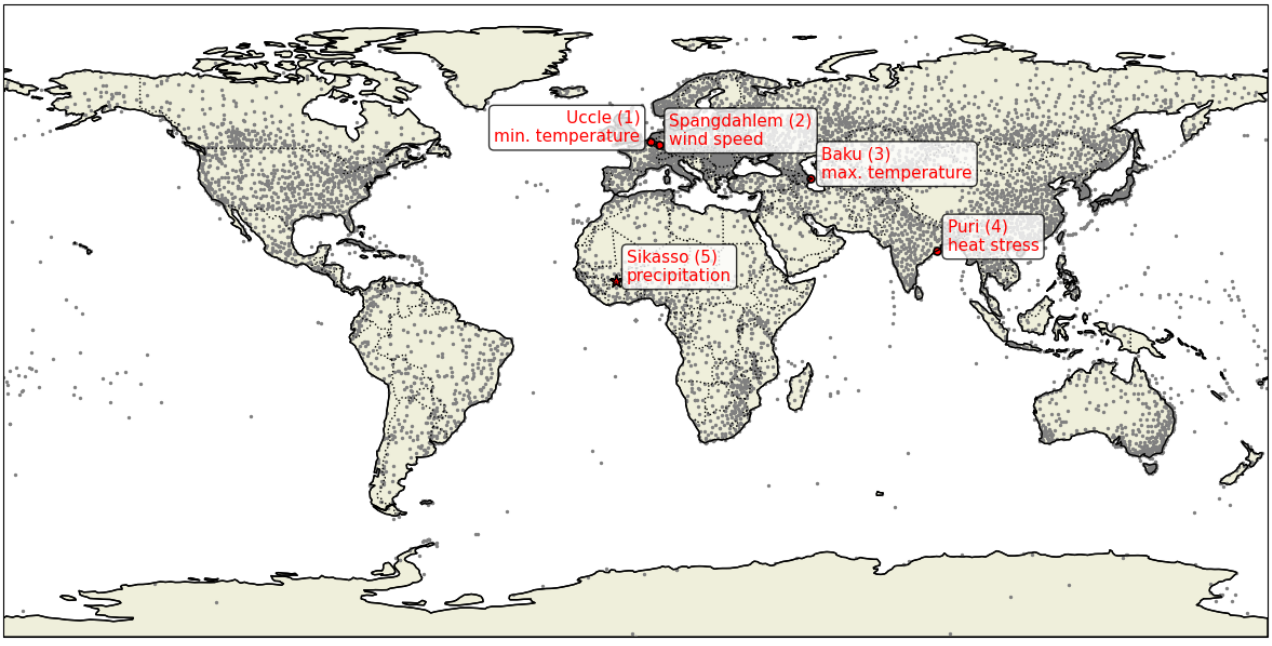

Figure 2. The 10010 stations from the global historical network (grey dots) of with it reports at least 30 years of data within the time span 1940–2023. EXSoDOS use cases for each of the variables provided by the global network are indicated as red circles and provided a user-input data as star for Sikasso (Mali).

by the user in a common format (csv, parquet, netcdf) for which one specifies their station coordinates (as elaborated by one of the use cases, see Sect. 2.6.2). Next, ERA5 (Hersbach et al., 2020) is used as reanalysis climate reconstruction for the coarse-scale predictor x_r. ERA5 reanalysis covers more than 80 years of data from 1940 until now that can be used for calibration and validation of the statistical model, hence suitable to build a robust statistical relation between predictor and predictand. Finally, the climate model ensemble members of the Coupled Model Intercomparison Project Phase 6 (CMIP6) see (Eyring et al., 2016) from 1931 up to 2100 are used as predictor input for EXSoDOS to generate and assess downscaled daily time series from past to future climate. These are downloaded from one of the data nodes of the Earth System Grid Federation (ESGF), see https://esgf.llnl.gov/. For demonstration of EXSoDOS, 9 models listed in the Tab. 1 are used, but the user can specify any other combination of model members available at ESGF.

2.2 Statistical downscaling

The basic model strategy is to randomly sample point-scale predictands (y) from measurements in such a way that they are correlating with coarse-scale predictors (x), as proposed by Switanek et al. (2022). As such, the predictors can be extracted from climate projection and then used as input for the model to generate future point-scale time series including future extreme values. The current method is now reformulated to work not only with precipitation but also with other climate parameters, including temperature, wind speed and heat stress. This is done by performing the normalizing and denormalization steps

https://doi.org/10.5194/egusphere-2025-2214
Preprint. Discussion started: 11 July 2025

Model	Member	Resolution	Reference
CanESM5	r1i1p1f1	$\sim 2.8^o \times 2.8^o$	Swart et al. (2019)
INM-CM4-8	r1i1p1f1	$\sim 1.5^o \times 2.0^o$	Volodin et al. (2018)
INM-CM5-0	r1i1p1f1	$\sim 1.5^o \times 2.0^o$	Volodin et al. (2017)
IPSL-CM6A-LR	r2i1p1f1	$\sim 2.5^o \times 2.5^o$	Boucher et al. (2020)
MIROC6	r1i1p1f1	$\sim 1.4^o \times 1.4^o$	Tatebe et al. (2019)
MPI-ESM1-2-LR	r10i1p1f1	$\sim 1.9^o \times 1.9^o$	Mauritsen et al. (2019)
MPI-ESM1-2-HR	r1i1p1f1	$\sim 0.9^o \times 0.9^o$	Gutjahr et al. (2019)
MRI-ESM2-0	r1i1p1f1	$\sim 1.1^o \times 1.1^o$	Yukimoto et al. (2019)
TaiESM1	r1i1p1f1	$\sim 1.25^o \times 1.25^o$	Lee et al. (2020)

Table 1. Climate models and references used in this study from the 6th phase of the Coupled Model Intercomparison Project (CMIP6), see Eyring et al. (2016).

with a non-parametric distributions. We further improve the model by implementing different predictor classes of different magnitude. Additionally, we implement a rescaling step of the point-scale predictand with the coarse-scale predictor before applying the stochastic model, which leads to improved results on high extremes in case of precipitation and wind speed (see Sect. 3.1 for results). For the sake of clarity, we elaborate the details of the statistical model in the subections below.

2.2.1 Stochastic model

A statistical relationship between x and y is established for each month separately. To increase the sample size and to make the transition between months more smooth, calibration data from the month before and the month after is taken into account as well.

Afterwards, to allow the relation between the predictor and predictand to be dependent on the magnitude of the predictor, the sample data is subdivided into a number of categories ($n = 3$) of different magnitudes of the predictor percentiles. In the case of temperature and heat stress, the category bins of equal sample size are constructed, for which their boundaries are determined by equidistant values of the cumulative distribution function $p(x)$:

$$p_i = i/n \text{ for } 0 \leq i \leq n \tag{1}$$

In the case of precipitation and wind speed, daily distributions have large tails, which we want to represent in the stochastic model. We use an exponential profile for quantiles of category borders which provides more categories in the tails:

$$p_i = \begin{cases} 1 - \exp(l_i) & \text{for } 0 \leq i \leq n-1 \\ 1 & \text{for } i = n \end{cases} \tag{2}$$

where

$$l_i = i \ln(f_{\max})/(n-1) \text{ for } 0 \leq i \leq n-1 \tag{3}$$

https://doi.org/10.5194/egusphere-2025-2214
Preprint. Discussion started: 11 July 2025

are equidistant values for i going from 0 to $n-1$, and $\ln(f_{\max})$ is the logarithm of the (prescribed) chance (that is, frequency $f_{\max}$)) for the observation to fall in the upper bin. As such, $p_{n-1} = 1 - f_{\max}$ represents the lower quantile border of that the upper bin. The exponential profile (note that $\ln(f_{\max})$ is negative hence also p_i) leads to more categories in the tails. Finally, the quantile categories q_i are calculated from the quantile function q_D of the calibration data x_r^c of the historical period (h):

$$q_i = q_{D^h_{x_r^c}}(p_i) \tag{4}$$

Here above and throughout this manuscript, we follow the notation of Maraun (2016). For each of these categories, the predictand is correlated with the predictor variable. At first, the predictor and predictands are normalized within each category for the calibration data:

$$\tilde{x}_r^c = q_N\left(p_{D_{x_r^c}}(x_r^c)\right) \tag{5}$$

$$\tilde{y}_o^c = q_N\left(p_{D_{y_o^c}}(y_o^c)\right) \tag{6}$$

where $p_{D_{x_r^c}}$ and $p_{D_{y_r^c}}$ are the cumulative distribution functions of the the calibration predictor x_r^c and predictand y_o^c, and q_N the quantile function of the normal distribution.

Subsequently, the correlation between the normalized predictor and normalized predictand is estimated from $\tilde{x}_r^c$ and $\tilde{y_o^c}$:

$$\rho_{\tilde{x}\tilde{y}} \simeq \langle \tilde{x}_r^c \tilde{y}_o^c \rangle \tag{7}$$

where $\langle \cdot \rangle$ indicates the average.

The normalized predictand is now sampled as a linear combination of normalized predictor and an extra random variable r as follows:

$$\tilde{y} = \alpha \tilde{x} + \beta \tilde{r} \tag{8}$$

with

$$\tilde{x} = q_N\left(p_{D_{x_r^c}}(x)\right) \tag{9}$$

the predictor normalized according to the estimated probability distribution function calculated above, and the predictor x can be either the upscaled reanalysis for validation x_r^v or the bias-adjusted climate models x_m for the application (predictor from climate projections). One can obtain $\tilde{y}$ correlating with $\tilde{x}$ with a correlation coefficient ρ by setting $\alpha = \rho$ and $\beta = \sqrt{1-\alpha^2}$ (see appendix A), hence

$$\tilde{y} = \rho \tilde{x} + \sqrt{1-\rho^2}\tilde{r} \tag{10}$$

Finally, one can calculate the modeled predictand by inverting Eq. 6:

$$y = q_{D_{y_o^c}}(p_N(\tilde{y})) \tag{11}$$

https://doi.org/10.5194/egusphere-2025-2214
Preprint. Discussion started: 11 July 2025

where p_N is the cumulative distribution function of the Gaussian normal distribution and $q_{D_{x^c}}$ is again the quantile function of the calibration dataset.

In contrast to Switanek et al. (2022), the current method for (de)normalizing the variables is non-parametric, hence doesn't take any assumptions on particular statistical distributions (eg., gamma distribution for precipitation or Weibull distribution for wind speed), hence any climate variable can be generated including precipitation, wind speed, temperature and heat stress, as long as the observation record is long enough to represent their density distributions.

2.2.2 Prescaling of predictand for precipitation and wind speed

The statistical relation described above is improved for precipitation and wind speed by rescaling the predictand with the predictor. Therefore, the equation 6 is modified as follows:

$$\tilde{y}_o^c = q_N\left(p_{D_{y_o^c}}(y_o'^c)\right) \tag{12}$$

with

$$y_o'^c = y_o^c/(c + x_r) \tag{13}$$

where c is a scale parameter that is set to 30 mm/day for precipitation and 2 m/s for wind speed, which avoids division by zero for $x_r = 0$. The modelled predictand given by Eq. 11 is then modified as follows:

$$y' = q_{D_{y_o'^c}}(p_N(\tilde{y})) \tag{14}$$

$$y = y' \cdot (c + x) \tag{15}$$

For values of $x >> c$, the correlated random sampling by Eqns. 10 and 14 is performed for the perturbation $y' \simeq y/x$ of the point-scale predictand from the coarse-scale predictor x instead of the point-scale predictand y itself. This leads to more robust results because it can be assumed that the expected value (ie., averaging over a large number of days for a particular value of x) of y approximately scales with the predictor x, or in other words, the expected value of y' is assumed to be a constant (and approximately 1). For values of $x << c$, the statistical model becomes equivalent to the original one by Eq. 11. This modification leads improved agreement of the modelled precipitation and wind speed with observed high extreme return periods of 1 to 10 years, as will be shown in the results section.

2.2.3 Detrending of climate projections

In the description above, a statistical relationship (ie., correlation through their normalized time series) is established between the predictor variable at the coarse scales and the predictand variable at the point scale. However especially in the case of temperature variables, distribution values in future climate at coarse scales exceed the range of the distribution of the historical period because of global warming. This leads to a cutoff for highest extremes, since they are all mapped to the highest observed value from the historical record. To overcome this problem and still represent the high extremes in future global warming, the predictor from the projections are detrended by dividing by the 30-year mean of the given month and multiplying it by its mean

https://doi.org/10.5194/egusphere-2025-2214
Preprint. Discussion started: 11 July 2025

of the reference period 1986–2015 (in order to avoid division by zero in this operation and the problems arising from negative values, temperature variables are expressed in Kelvin). This is done before normalizing the predictor in Eq. 9. Afterwards, the sampled predictand from Eq. 15 is retrended by dividing again by the predictor mean of the reference period and multiplying with the 30-year mean. By performing these operations, the statistical relationship (correlation) between the coarse-scale and point-scale variables is now considered relative to their long-term averages, and it's assumed that it doesn't change under climate change.

2.3 bias-adjustment of climate projections

In the previous section, a statistical model is constructed and calibrated on on historical reanalysis data used as predictor variables and the point-scale weather observations. To apply the statistical model to the climate projections as predictor, the consistency with the historical reanalysis needs to be maximized. Therefore, the raw CMIP6 ensemble climate model data is bias-adjusted against the historical reanalysis data with quantile delta-mapping. The latter is based on the quantile-delta mapping described in Cannon et al. (2015). For the sake of clarity, we elaborate the QDM correction below, in which we also follow the notation of Maraun (2016).

The model bias $B(p)$ is calculated as a function of the model's cumulative distribution function p (or 'p'robabilities corresponding to a given model quantile) with respect to the climate reconstruction x_r and the 'b'iased climate model output x_b^h in the historical overlapping timeframe (h) from 1961-2022:

$$B(p) = q_{D^h_{x_b}}(p) - q_{D^h_{x_r}}(p) \tag{16}$$

This bias function determines the difference between the quantiles $q_{D^h_{x_b}}(p)$ of the climate model output and those of the climate reconstruction $q_{D^h_{x_r}}(p)$. For the historical period, the time series bias is then calculated as follows:

$$B^h_{QDM}(x_{b,i}) = B\left(p_{D^h_{x_b}}(x_{b,i})\right) \tag{17}$$

from which can find the final bias-adjusted time series by subtracting the bias in the historical timeframe:

$$x_{m,i} = x_{b,i} - B^h_{QDM}(x_{b,i}) \tag{18}$$

for i a day in the historical time frame h (1991-2020). To create future bias-adjusted time series, quantile delta mapping assumes that the bias associated to each percentile $B(p)$ (while changing the timeframe for calculating each percentile) is invariant under climate change. We get the following bias-adjustment function for the future timeframe p:

$$B^p_{QDM}(x_{b,i}) = B\left(p_{D^p_x}(x_{b,i})\right) \tag{19}$$

and:

$$x_{m,i} = x_{b,i} - B^p_{QDM}(x_{b,i}) \tag{20}$$

https://doi.org/10.5194/egusphere-2025-2214
Preprint. Discussion started: 11 July 2025

for i a day in the projected timeframe p with a 30-year timespan (eg., 2071-2100). For a given day i, the timeframe for projection (p) is chosen in such a way that the day i is in the center of the timeframe. In practice, timeframes and the corresponding bias-adjustment function B^p_{QDM} are created in steps of five years, which is a compromise between computational cost and a smooth transition of bias-adjustment between the timeframes.

It can be verified that the cumulative density distribution of the climate model $\left(p_{D^p_{x_i}}\right)$ is re-evaluated in the future period, which ensures that climate change signals of the quantile distribution is conserved. This is because the quantiles in the respective historical and future cumulative distributions p undergo the same bias-adjustment $B(p)$, hence their difference remains conserved. This can be shown formerly by evaluating bias-adjustment (Eq. 20) on the quantiles $q_{D^p_{x_b}}(p)$ in the future timeframe:

$$\begin{aligned} q_{D_{x^p_m}}(p) &= q_{D^p_{x_b}}(p) - B_{QDM}\left(q_{D^p_{x_b}}(p)\right) \\ &= q_{D^p_{x_b}}(p) - B\left(p_{D^p_{x_b}}\left(q_{D^p_{x_b}}(p)\right)\right) \\ &= q_{D^p_{x_b}}(p) - B(p) \end{aligned} \tag{21}$$

and the bias-adjustment (Eq. 18) on the quantiles in the historical timeframe $q_{D^h_{x_b}}(p)$:

$$\begin{aligned} q_{D^h_{x_m}}(p) &= q_{D^h_x}(p) - B_{QDM}(q_{D^h_x}(p)) \\ &= q_{D^h_x}(p) - B(p_{D^h_x}(q_{D^h_x}(p)) \\ &= q_{D^h_x}(p) - B(p)) \end{aligned} \quad . \tag{22}$$

Subtracting the two equations shows that the climate change signal on the quantiles are invariant for the QDM correction:

$$q_{D_{x^p_m}}(p) - q_{D_{x^h_m}}(p) = q_{D^p_{x_b}}(p) - q_{D^h_{x_b}}(p) \tag{23}$$

bias-adjustment of climate models are calculated over continental or global grids at once. To lower the computational cost and to obtain a more smooth bias-adjustment function, the bias is calculated for discrete values l of the cumulative distribution function p_l. As such, the bias function can be approximated as follows:

$$B(p) \simeq \alpha(p)B(p_l) + (1-\alpha(p))B(p_{l+1}), \text{ for } l \text{ where } p_l \leq p < p_{l+1} \tag{24}$$

with

$$\alpha = (q - q_l)/(q_{i+l} - q_l) \tag{25}$$

As for the statistical model above, we consider equidistant discrete probability levels (in this case $n = 15$) for temperature-like and heat-stress metrics (see Eq. 1), and an exponential profile for precipitation and wind speed (see Eq. 2) to represent their big tails. The time series $p_{D^p_{x_b}}(x_b)$ are calculated from the model time series for each 5-year window and for each month separately, from which the bias at each timestep $B(p_{D^p_{x_b}}(x_b))$ can be evaluated using Eq. 24 and subtracted from the model output in Eq. 20.

As mentioned earlier, the climate models are generally coarser than the reference historical data, so the climate reconstruction (reanalysis data) is spatially aggregated to the coarser climate model grid. The bias may depend on the time of the year, hence

https://doi.org/10.5194/egusphere-2025-2214
Preprint. Discussion started: 11 July 2025

the bias-adjustment B is calculated for each month of the year separately. Hereby, the bias of each month is calculated by considering the month before, the month itself and the month after.

2.4 Validation of variability and extremes

Downscaled time series (y^v) are generated by applying the statistical model on the coarse-scale reanalysis predictor (x_r^v) over a climatological historical period (1961-2023), and validated with station observations y_o^v. The validation focusses on the representation of the variability and extreme events. Therefore, their annual cycles, density distributions and return levels as a function of return period for the different datasets and timeframes are compared with the observations. For the annual cycles, the mean, median and 10th-to-90th percentile range of each day throughout the year is provided for highlighting the combined seasonality and variability of each variable throughout the year. Magnitude of extreme events are highlighted with density distributions, whereas occurrence of extreme events are highlighted with return levels as a function of return periods. Density distributions for all variables are weighted so that their integral sums to unity. This is except for precipitation for which the density is weighted with the average precipitation, in such a way that the integral sums to the average annual precipitation. The advantage of such a weighted density is that extreme precipitation values become more visible on the plots. Herewith, we report the overlap area between the different density distributions (Devis et al., 2013; Perkins et al., 2007):

$$S = \int_{-\inf}^{+\inf} \min(PDF(y_v), PDF^o(y_v))dy_v \tag{26}$$

The return period, also known as a recurrence interval or repeat interval, is a commonly used metric in extreme (weather) analysis that evaluates the average time between subsequent extreme events of a certain magnitude or return level. To show high extremes for daily maximum temperature, precipitation, wind speed and heat stress, return levels are determined that is exceeded as a function of the return period. To quantify low extremes for daily minimum temperature, we determine the return level that is subceeded (ie., becomes lower than the return level) as a function of the return period. In theory, the model can be validated for any return period, but this depends on the length of the observation record. To only retain retain statistically relevant results for the current validation period 1961-2023, we only show return periods of up to 5 years which lead to an averaging over least 6 validation samples per return period over the 63 year period, ie., 63 years divided by five years, and divided by two since only half of the measurements are used for the validation.

All variables are extracted and processed directly from the respective data sources. This is except for heat stress. For the latter, we use the heat-stress temperature as proposed by Wouters et al. (2022):

$$T_s = T_w + 4.5\left(1 - \left[\frac{RH}{100}\right]^2\right) \tag{27}$$

which adjusts the wet-bulb temperature T_w to reflect the association with heatwave mortality under different levels of relative humidity (RH) and temperature.

https://doi.org/10.5194/egusphere-2025-2214
Preprint. Discussion started: 11 July 2025

2.5 Climate-change assessment of variability and extremes

For the climate change assessment, downscaled time series (y) are generated by applying the statistical model on multiple bias-corrected climate models as coarse-scale predictor (x_m). We show 10th-to-90th percentile ensemble spread of density distributions and return levels over the 9 different models member from CMIP6 (see Tab. 1). To demonstrate EXSoDOS, we show results from the Shared Socio-economic Pathway for fossil fueled development with $8.5\mathrm{Wm}^{-1}$ radiative forcing (SSP585), see IPCC (2021). The user can change to other SSP scenarios to assess future climate uncertainties. Results are shown for three 30-year time frames, one for the future (2071-2100), and two past periods (1961-1990 and 1991-2020). For the two past periods, results from observations are also added to compare the past shifts of modeled weather extremes to the observations, and then assess whether and how these shifts would continue in the future.

2.6 Use cases

2.6.1 Use cases based on NOAA data archive

To show the general utility of EXSoDOS according to particular local challenges of climate change, we apply and evaluate EXSoDOS for 5 cases across the globe. For each of these locations we show the results of one variable according to a particular local challenge of climate change (for their locations, see Fig. 2). For Uccle (Belgium) in Europe, one of the challenges facing climate change is that many native vegetation (crop) species require the occurrence of freezing temperatures to be able to blossom in spring, hence minimum daily temperature is demonstrated for this location. For Spangdalhem (Germany) also in Europe, the power yield of a cluster of wind turbines depends on the distribution of wind, hence for this location we show results for daily wind speed. The Middle-East and the region of South-Causassus around the Caspian Sea contains one of the hot spots of high temperature of the world, see for example Fig. 1D of Wouters et al. (2022). Therefore, we assess daily maximum temperature of climate change on extremely high temperature For Baku (Azerbaijan) where COP29 took place in November '24. Finally, Large parts of India are exposed to extreme heat stress due a combination of high temperature and humidity, see for example Fig 1C of Wouters et al. (2022). We exemplify EXSoDOS by showing results of heat stress temperature Wouters et al. (2022) for Puri located along the east coast of India. For the use case locations above, measurement data are extracted from the NOAA archive (see section 2.1), highlighting the applicability of EXSoDOS for any location with measurements in this archive.

2.6.2 Use case based on local data by MALI-METEO

Mali, located in West Africa, is characterized by Sahelian and semi-arid climate. In Mali, rainfall is concentrated in the south part, with more intense and regular rainfall, while it decreases as it moves northwards, where it becomes scarce. The data used in this study are ground observations of daily rainfall times series from the MALI-METEO database for the period 1961 to 2023 from the Sikasso synoptic station (Latitude: 11°19'N, Longitude: 05°41'W, Altitude: 415.05m).

https://doi.org/10.5194/egusphere-2025-2214
Preprint. Discussion started: 11 July 2025

As rainfall is a dichotomous variable, its inter-annual variability in time and space is difficult to assess. Rainfall is a key element in Mali, and particularly in Sikasso, playing a crucial role in agriculture, which is the main source of subsistence for the local population. However, its variability has a direct impact on crop yields and the availability of water resources and exacerbates the vulnerability of communities to climatic hazards. Daily times series of rainfall in Sikasso station clearly show that the rainfall pattern in this locality is unimodal, with a more intense character in August. In fact, the absolute record for 24h cumulative rainfall in Sikasso is 166.1mm, observed on August 12, 1963. Sikasso is a region where large quantities of rain are observed every year. In 2023, flooding caused the loss of 123.5 hectares of agricultural land and affected 4,023 people, including 2 deaths (Source: Annual report of the Direction Générale de la Protection Civile, 2023). However, in 2024, the impact of flooding increased considerably, with 7,017 hectares of agricultural land lost and 4,231 people affected (Source: Annual report of the Direction Générale de la Protection Civile, 2024).

To demonstrate the applicability of EXSoDOS on locally supplied observations as an alternative to the NOAA database, observations from MALI-METEO in Sikasso were used. Also, this use case was experimented during an interactive workshop on weather and climate data (“ L’engagement des parties prenantes nationales dans la formulation de politiques agricoles précises pour des stratégies d’adaptation au changement climatique au Mali”) held from October 21 to 25, 2024 in Bamako (Mali) with an online Jupyter Notebook, see Carter (2024).

3 Results

3.1 Validation of downscaling reanalysis

We first validate the statistical downscaling algorithm by applying it on the validation predictor x_r^v (upscaled ERA5) and compare its output with the observed predictand y_o^v. for the historical period 1961–2023. This is done for the different meteorological quantities in different study areas described in section 2.6. Annual cycles, distributions and return period for each of the case studies are shown in Figs. 3, 4 and 5. Overall, ERA5 matches well the average annual cycles of the observations over multiple years for each variable (Fig. 3). However, the annual cycles of ERA5 underrepresent the variability over years, as highlighted by the 10-to-90 percentile range of each day of the year in Fig. 3. This is especially the case for precipitation in Sikasso (Mali), for which both dry days and extreme high precipitation are underrepresented. The underrepresentation is more subtle for the temperature variables, such as daily minimum temperature for Uccle in Belgium and the daily maximum temperature for Baku (Azerbaijan), and for heat stress temperature for Puri (India). The underrepresentation of extremes is more pronounced when ERA5 is upscaled to a coarser resolution of global climate models (1^o resolution), as extreme values are averaged out over larger grid sizes. In contrast, all results for ERA5 downscaled to the station level match better the variability of the annual cycle compared to the original ERA5. The improved representation of extremes by downscaling becomes more clear when analyzing density distributions 4 and return periods 5. Distributions of precipitation after downscaling are better matching the observations (thin dashed line versus thick dashed line) than without downscaling of ERA5 (thick line versus thin dashed line), since they get shifted to more high extremes, while also the number of dry days becomes larger and better matching observations (Fig. 4). At the same time, the downscaling also reduces the overall bias in annual precipitation for Sikasso

https://doi.org/10.5194/egusphere-2025-2214
Preprint. Discussion started: 11 July 2025

where the downscaled value (1210 mm) is closer to the observed value (1205 mm) than ERA5 value (842 mm). Other variables, particularly daily minimum and maximum temperature, wind speed and heat stress, also show a better match with the observed distribution after downscaling with larger spread (Fig. 4). The Perkins distribution overlap scores (Eq. 26) confirms the better match of the distributions after downscaling, showing higher scores for each variable, see Tab. 3. All downscaled variables

Table 2. Perkins distribution overlap scores (Eq. 26) for different variables and locations.

Variable (Location)	Dataset	Score
Daily minimum temperature (Uccle, Belgium)	ERA5 DS	0.986
	ERA5 orig	0.941
	ERA5 upscaled	0.943
Wind speed (Spangdahlem, Germany)	ERA5 DS	0.963
	ERA5 orig	0.709
	ERA5 upscaled	0.631
Daily maximum temperature (Baku, Azerbaijan)	ERA5 DS	0.971
	ERA5 orig	0.929
	ERA5 upscaled	0.746
Heat stress temperature (Puri, India)	ERA5 DS	0.978
	ERA5 orig	0.951
	ERA5 upscaled	0.894

Table 3. Perkins distribution overlap scores (Eq. 26) for the downscaled ERA5 (ERA5 DS), original ERA5 (ERA5 orig), and upscaled ERA5 (ERA5 upscaled)

(including daily minimum temperature) show more extreme levels for the high return periods compared to original ERA5 data, for which they approximate the return levels of the observations much better (Fig. 5). We also highlight that prescaling of the predictand with predictor (see Eq. 12 and 15) leads to more consistency of the model results with extreme observations than without the prescaling (see Eq. 6 and 11) especially for precipitation, compare bottom panel of Fig. 5 compared to Fig. 1 of supplementary material.

3.2 Assessment of extremes under climate change

In this section, assessment is demonstrated for each of the variables for the different areas under the SSP585 scenario by comparing results of a 30-year timeframe by the end of the century (2071-2100) and of two 30-year timeframes of in the past 1961-1990 and 1991-2020, see Figs. 6 and 7. Overall, there is a tendency towards higher (extreme) values for the original climate projections (CMIP6) (Fig. 6) towards the future (green versus grey lines). This is except for daily wind speed and for minimum temperature, the low values become less extreme. For daily and maximum temperature, precipitation and heat stress, the variables bias-corrected and downscaled from CMIP6 (CMIP6_BC_DS) could better capture the tendencies between

https://doi.org/10.5194/egusphere-2025-2214
Preprint. Discussion started: 11 July 2025

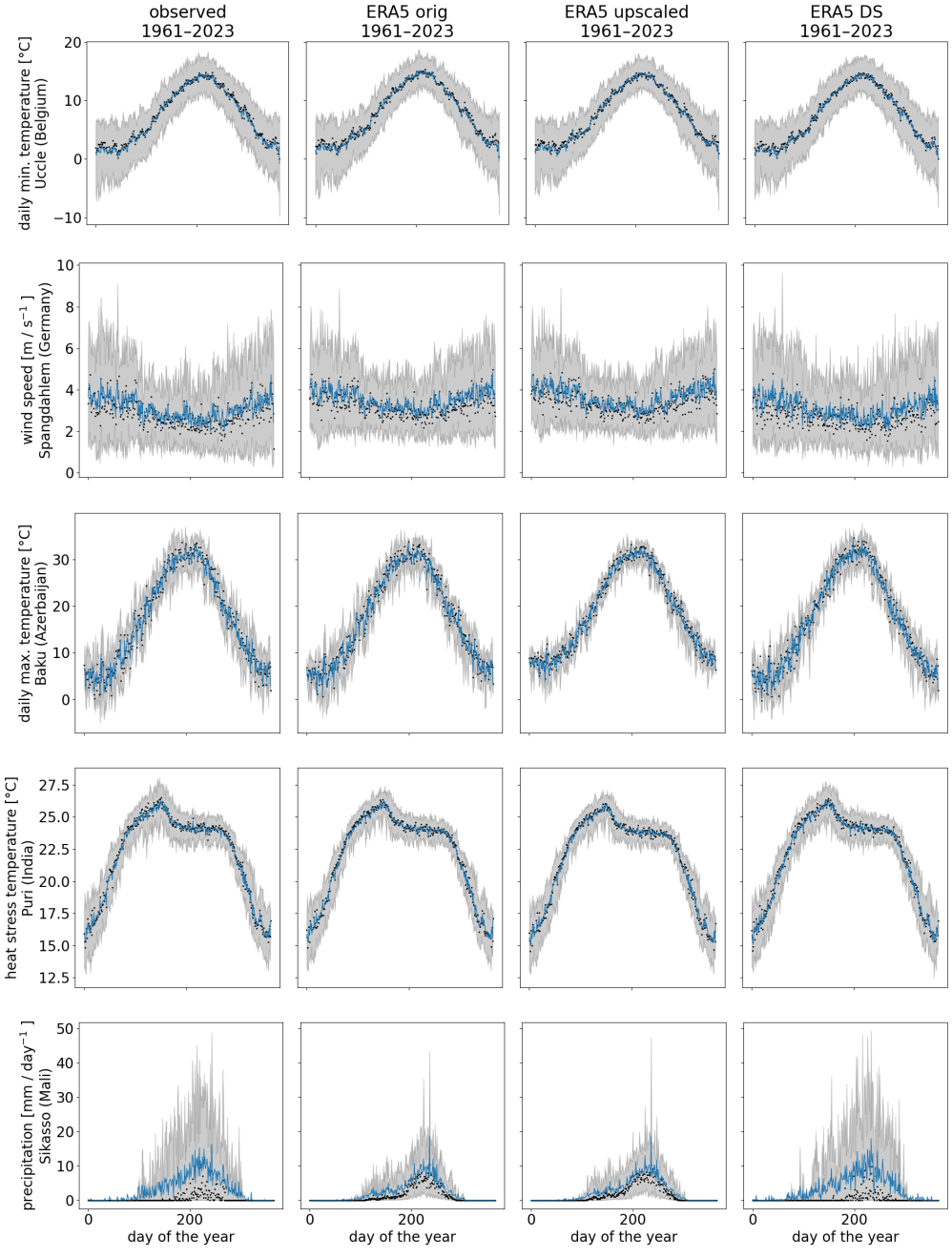

Figure 3. Annual cycles from observations for the period (1961-2023), ERA5 on its original grid (ERA5 orig), ERA5 upscaled to the grid of a climate model (ERA5 upscaled), and ERA5 downscaled with the statistical model (ERA5 DS). The blue lines indicate the average, whereas the black dots show the median of each day of the year over the multiple years. The grey bars indicate the range between the 10th and 90th percentile values over the different years. We show daily minimum temperature for Uccle in Belgium (first row), daily mean wind speed for Dahlem in Germany (second row), daily maximum temperature for Uccle in Belgium (third row), heat stress temperature for Puri in India (fourth row), and precipitation for Sikasso in Mali (last row).

https://doi.org/10.5194/egusphere-2025-2214
Preprint. Discussion started: 11 July 2025

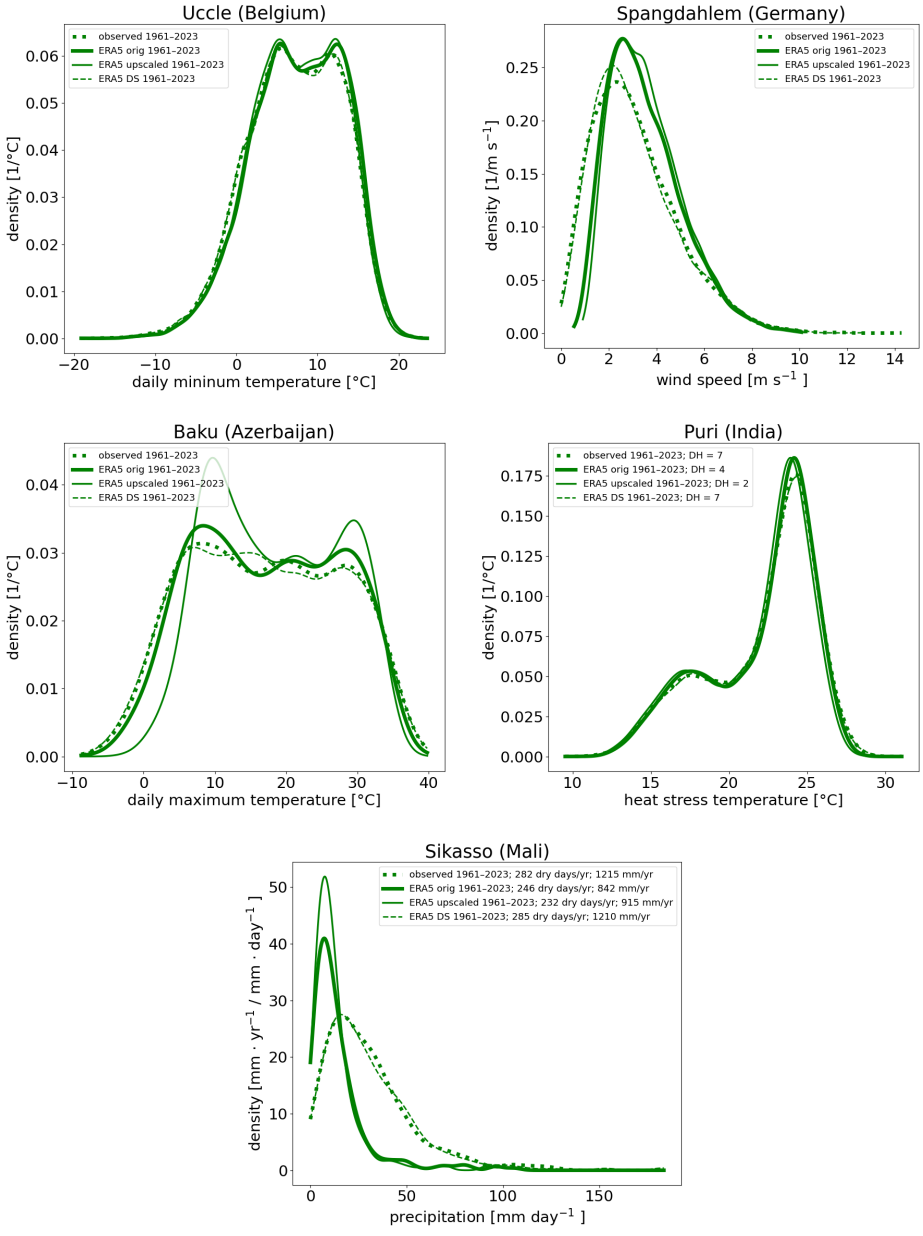

Figure 4. Density distribution from daily observations for the period (1961-2023), ERA5 on its original grid (ERA5 orig), ERA5 upscaled to the grid of a climate model (ERA5 upscaled), and ERA5 downscaled with the statistical model (ERA5 DS). We show daily minimum temperature for Uccle in Belgium (upper left panel), daily mean wind speed for Dahlem in Germany (upper right panel), daily maximum temperature for Uccle in Belgium (center left panel), heat stress temperature for Puri in India (center right panel), and precipitation for Sikasso in Mali (lower panel). For precipitation, the annual number of dry days and the annual precipitation are provided, and for heat stress temperature the annual number of deadly heat days (heat stress temperature $> 27°C$)

https://doi.org/10.5194/egusphere-2025-2214
Preprint. Discussion started: 11 July 2025

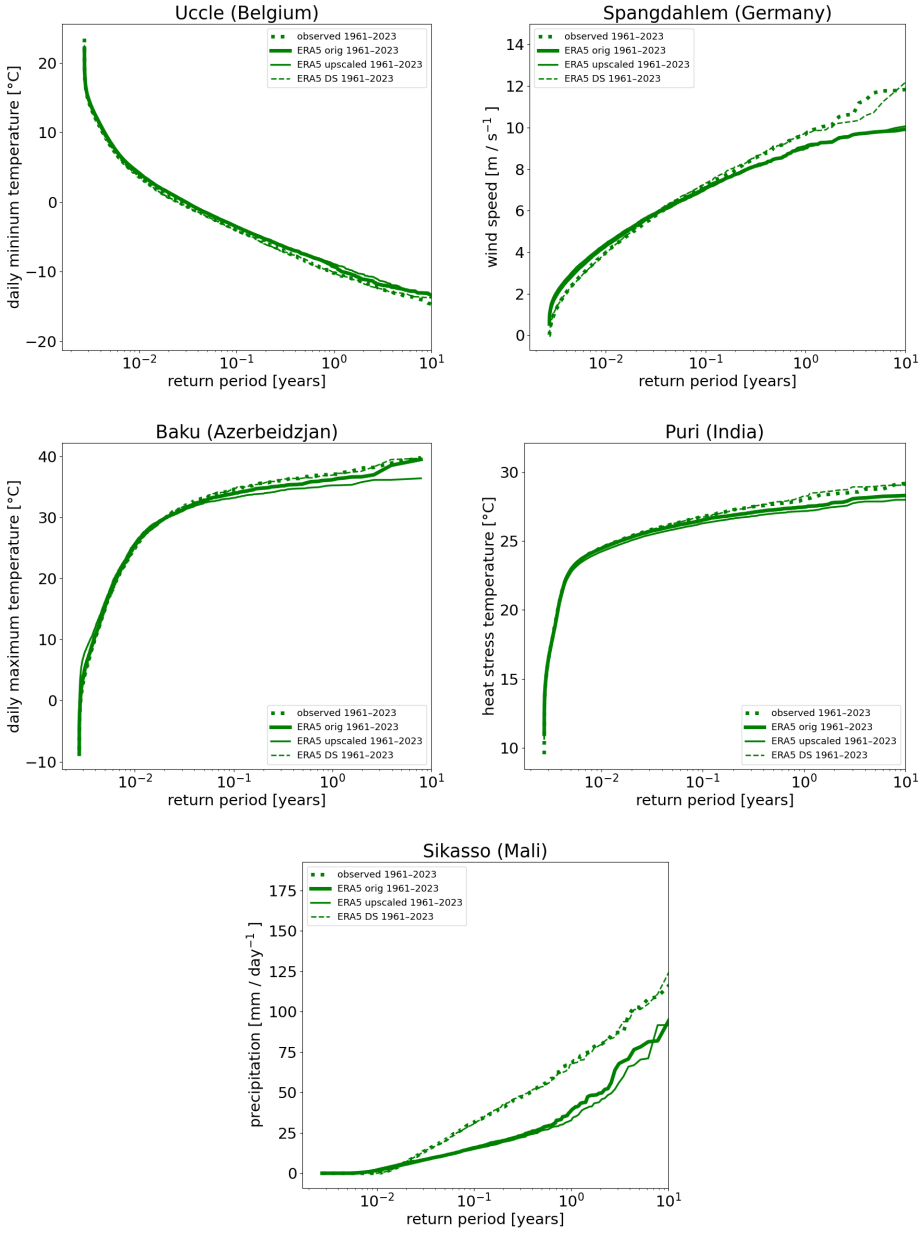

Figure 5. Idem as Fig. 4, but for return levels.

https://doi.org/10.5194/egusphere-2025-2214
Preprint. Discussion started: 11 July 2025

the two past periods than the original CMIP6 (thin green line versus thin grey line). A shift towards more extremes is already present in the original CMIP6 data (thin green line versus thin grey line) but the distributions have a substantial bias, just like the ERA5 values (both the original and upscaled to the climate model) as discussed in the previous section. Especially, the extremes in CMIP6 have an overall bias as discussed in the previous section, and this is also found for the shift under climate change. Thanks to the bias-correction and downscaling, the observed values and their shift under climate change are now captured by biascorrected and downscaled CMIP6 (thick green line versus thick grey line), see Fig. 6. Particularly for precipitation (Sikasso), an overall underestimation of dry days and high extreme values are found for CMIP6 (see numbers in lower panel of Fig. 6), as also found for ERA5 (original and upscaled) as shown in the previous section. The shift of precipitation distribution by CMIP6 also tends to be underestimated (thin green lines versus thin grey lines in Fig. 6), as well as their return values and their shifts (Fig. 7). The underestimation in absolute values and their shifts is largely alleviated by employing the downscaling on bias-corrected CMIP6 (CMIP6_BC_DS), see Figs. 6 and 7. This is the case for all shifts in return periods, except for those of precipitaton between two and six years. For the latter, there is a slight decrease in the observations while the downscaled values still show an increase. Daily minimum temperature (Uccle), daily maximum temperature (Baku) and heat stress temperature (Puri) all tend to be overestimated by CMIP6, and these biases are all largely alleviated by CMIP6_BC_DS, see Figs. 6 and 7. After this alleviation, it becomes clear that historical tendencies are well represented. For wind speed for Spangdahlem however, the overall distributions of the observations are captured well, but the shift in the observations is not predicted, since large-scale wind speed distribution (CMIP6) doesn't show a shift either.

The tendencies of having higher extremes (except for wind speed) pull through to the end of the 21st century under the SSP585 scenario, see 6 and 7. While original CMIP6 ensemble precipitation already indicates a tendency towards more extremes in the future, the downscaled ensemble (CMIP6_BS_DS) substantially from the original CMIP6 ensemble both in absolute and relative numbers. For precipitation return periods between 0.1 and 1 year, for example, an average increase from 17.1/day to 31.0/day, hence an increase of 13.9mm/day (∼81%), is found for the raw CMIP6. At the same time, an average increase from ∼43.3mm/day to ∼57.2mm/day is found for CMIP6_BS_DS, hence an increase of ∼14.4mm/day (∼33%). A discrepancy also exists in terms of return periods: an event with a return period of 1 year according to CMIP6 ($\geq$ 32.0mm/day) would have a return period 0.247 (∼1/4) year in a future climate, whereas an event with a return period of 1 year according to CMIP6_BC_DS ($\geq$ 69.1mm/day) would have a return period of 0.349 (∼1/3) year. Future temperature, heat stress and wind speed are also affected after downscaling. For heat stress, the (change in) number of days with extreme heat is higher after downscaling than from the original CMIP6 ensemble, see Fig. 7. These results highlight that different types of climate-change assessments using downscaled GCM output leads to different results than those using original GCM output.

4 Conclusions

A downscaling method EXSoDOS is developed for the DOwnscaling of local weather EXtremes Shifts under global warming, including daily minimum and maximum temperature, precipitation, heat stress and wind speed. The model employs ground-based measurements, historical reanalysis climate reconstruction and ensemble climate projections as input. Stochastic mod-

https://doi.org/10.5194/egusphere-2025-2214
Preprint. Discussion started: 11 July 2025

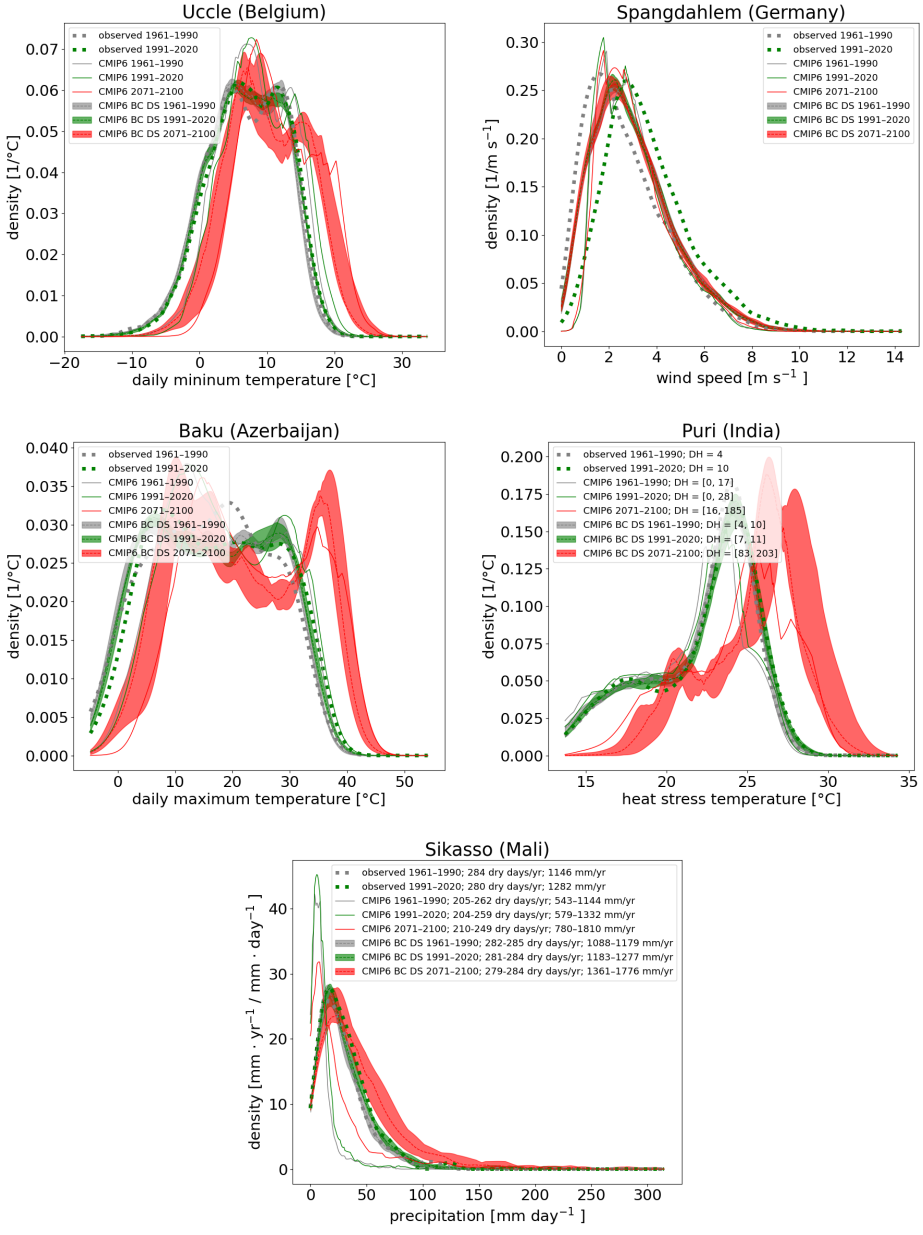

Figure 6. Idem as Fig. 4, but showing results for original CMIP6 climate projections (SSP585) including models listed in Tab. 1, bias-corrected and downscaled CMIP6 models (CMIP6_BC_DS). Observations and downscaled ERA5 are also included as comparison. Results are shown for two historical time frames 1961–1990 (in grey) and 1991–2020 (green), and for one future timeframe 2071–2100 (in red). For CMIP6_BS_DS, we show the 10-to-90 percentile spread over the different models.

https://doi.org/10.5194/egusphere-2025-2214
Preprint. Discussion started: 11 July 2025

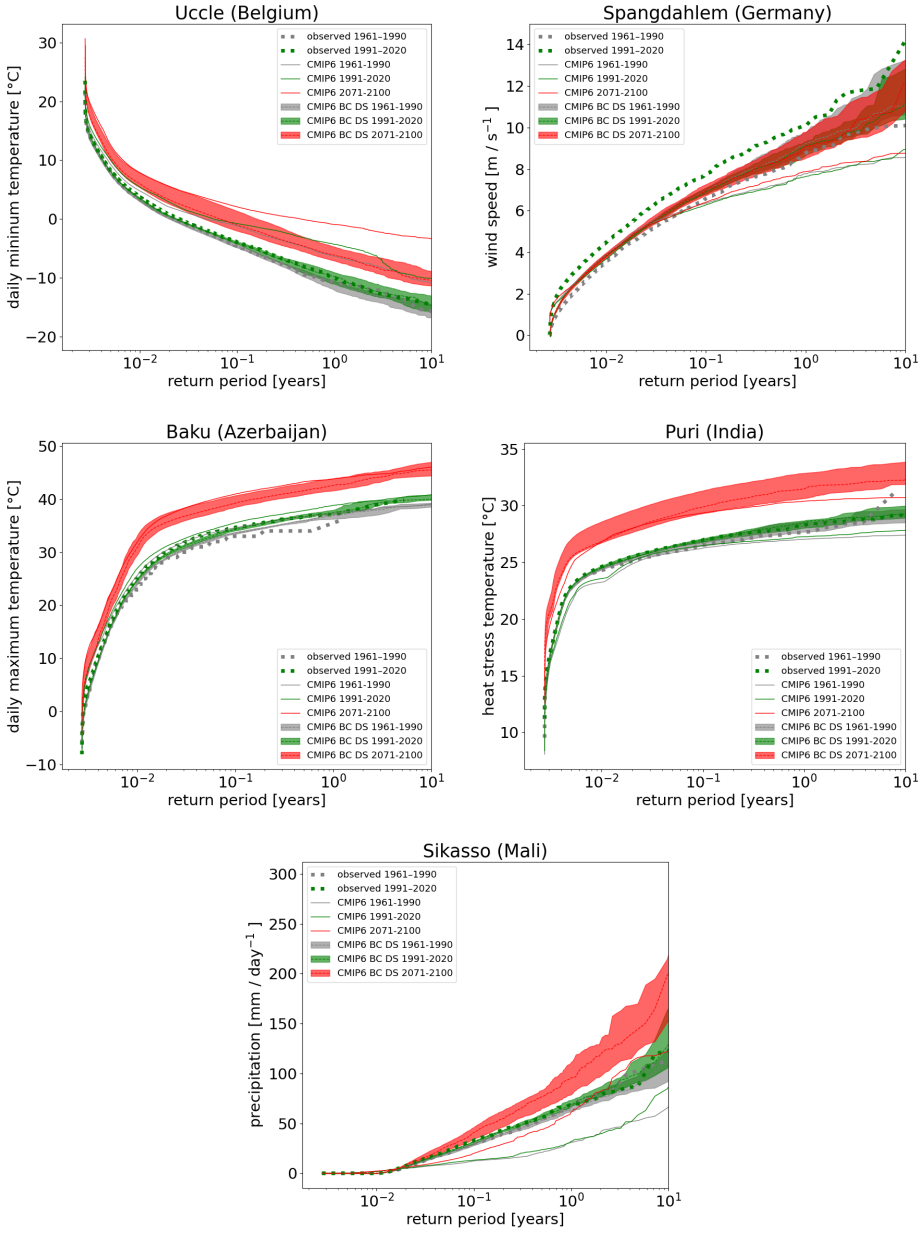

Figure 7. Idem as 6, but for the return levels.

https://doi.org/10.5194/egusphere-2025-2214
Preprint. Discussion started: 11 July 2025

elling is performed by normalizing the local measurements and coarse climate reconstruction and determining the monthly correlation between them for 3 categories of magnitude. Afterwards, the correlation function is applied to different bias-corrected climate model members. The framework uses measurements from the data archive maintained by NOAA (National Oceanic and Atmospheric Administration; https://www.ncei.noaa.gov/pub/data/, the ERA5 reanalysis data from C3S (Copernicus Climate Change Service; https://cds.climate.copernicus.eu) and CMIP6 climate projections from ESGF (Earth System Grid Federation; https://esgf-node.llnl.gov/esg-search). One can also provide its custom measurement data as alternative observation input, as long as the data has climatological coverage of multiple tens of years.

Each of the extreme weather variables are tested for particular case areas around the world where records are available on climatological time scales. They include daily minimum temperature for Uccle (Belgium), daily maximum temperature for Baku (Azerbaijan), heat stress temperature for Kasungu (Malawi), wind speed for Dahlem (Germany), and daily precipitation in Sikasso (Mali). For these case studies, EXSoDOS was found to reproduce the annual cycle statistics (climatological mean, median and 10th-to-90th percentile range), the density distribution and return periods. The high skill of the model to reproduce extreme occurrences up to 10 year return periods is achieved by the two-step bias-correction and downscaling procedure in line with previous methods (Switanek et al., 2022; Volosciuk et al., 2017). The results for extreme precipitation and wind speed, especially for occurrences of 1 to 10-year return periods, are further improved by the additional prescaling of the point-scale predictand with the coarse-scale predictor, hence for which high extremes are sampled as a perturbation of the grid-scale predictor.

EXSoDOS was also able to reproduce many of the observed shifts in extreme weather of the past climate (1991-2020 versus 1961-1990), including a tendency to more extreme precipitation and more extreme high temperature and heat stress, and a reduction in cold extremes. While the overall statistics of wind speed were found to be reproduced, the shift in more extreme wind in the observations was not found in CMIP6 or the downscaled time series. Applying the model on future climate projections towards the end of the 21st century (2071-2100), it was found that increasing extremes for daily maximum temperature, precipitation and heat stress are all exacerbated under future global warming. We further show that outcomes of shifting climate extremes are affected in different ways when applying a downscaling. Particularly for precipitation, relative and absolute climate-change signals are affected, as well as the changing return periods. As such, EXSoDOS downscaling is able to offer a baseline estimation of weather extremes and their past and future shifts under global warming for multiple weather variables for the first time, for which the statistical model is constrained with observations at any location on Earth where climatological measurements are available. Since the algorythm has a low computational cost and uses globally available data, its application could be upscaled to perform assessments for the available data archive of weather stations accross the globe (see Fig. 2), but also for single assessments with available data by local institutes.

One should keep in mind the limitations of statistical downscaling when employing the model for future climate assessment. Shifts of local extremes rely on the realism of the shifts the climate variables at the coarse scale provided by the global climate models, and on the representativeness of the correlation function established between the coarse-scale variable (predictor) and point-scale variable (predictand). Particularly, the correlation is considered static, while in reality this correlation may change under global warming. The stochastic model considers only one predictor at a particular location at a time, while local

https://doi.org/10.5194/egusphere-2025-2214
Preprint. Discussion started: 11 July 2025

extremes may be associated by the anomalies of multiple large-scale variables. As such, complexity of physical processes may be underrepresented by the model, and considering compound events of different variables at neighbouring locations is not possible. In order to perform a more in-depth analysis of changing extremes and their underlying physics, one should still employ mechanistic high-resolution atmospheric numerical modelling.

The accuracy of the stochastic model could be improved by considering multiple coarse-scale predictors and predictands at different locations simultaneously. This would not only allow the improve the physics, but also the consideration of compound events. This is possible by upgrading with correlation matrices among the predictands and predictors. Finally, in order to improve the representation of underlying drivers and their shifts under global warming, the correlation function could be upgraded with artificial intelligence.

Code and data availability. The code with documentation (README.md) and input data can be accessed on Zenodo at https://doi.org/10.5281/zenodo.15387101 (Wouters, 2025).

Appendix A: Random sampling of a variable correlating with another

We look for α and β in such a way that $\tilde{y}$ correlates with $\tilde{x}$ with correlation coefficient ρ estimated from the calibration above.

$$\begin{aligned} \rho &= \langle \tilde{y}\tilde{x} \rangle \\ &= \langle \alpha x x \rangle + \langle \beta r x \rangle \\ &= \alpha \sigma_x^2 \\ \rho &= \alpha \end{aligned} \tag{A1}$$

where $\sigma_{\tilde{x}} = 1$

$$\begin{aligned} \sigma_y^2 &= \langle yy \rangle \\ &= \langle (\alpha x)^2 \rangle + \langle 2\alpha x \beta r \rangle + \langle (\beta r)^2 \rangle \\ &= \alpha^2 \sigma^2 + \beta^2 \sigma_r^2 \\ &= \alpha^2 + \beta^2 \end{aligned} \tag{A2}$$

where $\sigma_y = \sigma_x = 1$. So

$$\beta = \sqrt{1 - \alpha^2} \tag{A3}$$

Author contributions. H.W. led the writing of the original draft, conceptualized the study, developed the methodology, performed formal analysis, and contributed to visualization. J.B. contributed to conceptualization and reviewed and edited the manuscript. F.P. acquired funding, administered the project, and performed validation. B.D. curated data, provided resources, contributed to validation, and reviewed and edited

https://doi.org/10.5194/egusphere-2025-2214
Preprint. Discussion started: 11 July 2025

the manuscript. A.D. curated data, provided resources, contributed to validation, and reviewed and edited the manuscript. R.H. developed software and provided resources. D.L. contributed to conceptualization and supervised the research.

Competing interests. The authors declare that they have no conflict of interest.

Acknowledgements. This used data has been collected and analyzed within the project "StratAdapt", funded by the Government of Flanders through the Flanders International Climate Action Programme (IKF 22/081). The authors thank Dr. Folorunso Akinseye and the organizations MALI-METEO and ICRISAT-Mali for their supporting role in data collection and acquisition during the course of the StratAdapt-Mali Project.

https://doi.org/10.5194/egusphere-2025-2214
Preprint. Discussion started: 11 July 2025

References

Weather and Climate Extreme Events in a Changing Climate, in: Climate Change 2021 – The Physical Science Basis: Working Group I Contribution to the Sixth Assessment Report of the Intergovernmental Panel on Climate Change, edited by Intergovernmental Panel on Climate Change (IPCC), pp. 1513–1766, Cambridge University Press, Cambridge, ISBN 978-1-009-15788-9, https://doi.org/10.1017/9781009157896.013, 2023.

Boucher, O., Servonnat, J., Albright, A. L., Aumont, O., Balkanski, Y., Bastrikov, V., Bekki, S., Bonnet, R., Bony, S., Bopp, L., Braconnot, P., Brockmann, P., Cadule, P., Caubel, A., Cheruy, F., Codron, F., Cozic, A., Cugnet, D., D'Andrea, F., Davini, P., De Lavergne, C., Denvil, S., Deshayes, J., Devilliers, M., Ducharne, A., Dufresne, J.-L., Dupont, E., Éthé, C., Fairhead, L., Falletti, L., Flavoni, S., Foujols, M.-A., Gardoll, S., Gastineau, G., Ghattas, J., Grandpeix, J.-Y., Guenet, B., Guez, E., L., Guilyardi, E., Guimberteau, M., Hauglustaine, D., Hourdin, F., Idelkadi, A., Joussaume, S., Kageyama, M., Khodri, M., Krinner, G., Lebas, N., Levavasseur, G., Lévy, C., Li, L., Lott, F., Lurton, T., Luyssaert, S., Madec, G., Madeleine, J.-B., Maignan, F., Marchand, M., Marti, O., Mellul, L., Meurdesoif, Y., Mignot, J., Musat, I., Ottlé, C., Peylin, P., Planton, Y., Polcher, J., Rio, C., Rochetin, N., Rousset, C., Sepulchre, P., Sima, A., Swingedouw, D., Thiéblemont, R., Traore, A. K., Vancoppenolle, M., Vial, J., Vialard, J., Viovy, N., and Vuichard, N.: Presentation and Evaluation of the IPSL-CM6A-LR Climate Model, Journal of Advances in Modeling Earth Systems, 12, e2019MS002 010, https://doi.org/10.1029/2019MS002010, 2020.

Brisson, E., Demuzere, M., Willems, P., and Van Lipzig, N. P. M.: Assessment of Natural Climate Variability Using a Weather Generator, Climate Dynamics, 44, 495–508, https://doi.org/10.1007/s00382-014-2122-8, 2015.

Brisson, E., Van Weverberg, K., Demuzere, M., Devis, A., Saeed, S., Stengel, M., and Van Lipzig, N. P. M.: How Well Can a Convection-Permitting Climate Model Reproduce Decadal Statistics of Precipitation, Temperature and Cloud Characteristics?, Climate Dynamics, 47, 3043–3061, https://doi.org/10.1007/s00382-016-3012-z, 2016.

Cannon, A. J., Sobie, S. R., and Murdock, T. Q.: Bias Correction of GCM Precipitation by Quantile Mapping: How Well Do Methods Preserve Changes in Quantiles and Extremes?, Journal of Climate, 28, 6938–6959, https://doi.org/10.1175/JCLI-D-14-00754.1, 2015.

Carter, T.: StratAdapt: Advancing Climate-Resilient Agriculture in Mali, https://pressroom.icrisat.org/stratadapt-advancing-climate-resilient-agriculture-in-mali, 2024.

Coppola, E., Raffaele, F., Giorgi, F., Giuliani, G., Xuejie, G., Ciarlo, J. M., Sines, T. R., Torres-Alavez, J. A., Das, S., Di Sante, F., Pichelli, E., Glazer, R., Müller, S. K., Abba Omar, S., Ashfaq, M., Bukovsky, M., Im, E.-S., Jacob, D., Teichmann, C., Remedio, A., Remke, T., Kriegsmann, A., Bülow, K., Weber, T., Buntemeyer, L., Sieck, K., and Rechid, D.: Climate Hazard Indices Projections Based on CORDEX-CORE, CMIP5 and CMIP6 Ensemble, Climate Dynamics, 57, 1293–1383, https://doi.org/10.1007/s00382-021-05640-z, 2021.

De Ridder, K., Lauwaet, D., and Maiheu, B.: UrbClim – A Fast Urban Boundary Layer Climate Model, Urban Climate, 12, 21–48, https://doi.org/10.1016/j.uclim.2015.01.001, 2015.

Devis, A., van Lipzig, N. P. M., and Demuzere, M.: A New Statistical Approach to Downscale Wind Speed Distributions at a Site in Northern Europe, Journal of Geophysical Research: Atmospheres, 118, 2272–2283, https://doi.org/10.1002/jgrd.50245, 2013.

Eyring, V., Bony, S., Meehl, G. A., Senior, C. A., Stevens, B., Stouffer, R. J., and Taylor, K. E.: Overview of the Coupled Model Intercomparison Project Phase 6 (CMIP6) Experimental Design and Organization, Geoscientific Model Development, 9, 1937–1958, https://doi.org/10.5194/gmd-9-1937-2016, 2016.

Fosser, G., Gaetani, M., Kendon, E. J., Adinolfi, M., Ban, N., Belušić, D., Caillaud, C., Careto, J. A. M., Coppola, E., Demory, M.-E., De Vries, H., Dobler, A., Feldmann, H., Goergen, K., Lenderink, G., Pichelli, E., Schär, C., Soares, P. M. M., Somot, S., and Tölle, M. H.:

https://doi.org/10.5194/egusphere-2025-2214
Preprint. Discussion started: 11 July 2025

Convection-Permitting Climate Models Offer More Certain Extreme Rainfall Projections, npj Climate and Atmospheric Science, 7, 51, https://doi.org/10.1038/s41612-024-00600-w, 2024.

Gutjahr, O., Putrasahan, D., Lohmann, K., Jungclaus, J. H., Von Storch, J.-S., Brüggemann, N., Haak, H., and Stössel, A.: Max Planck Institute Earth System Model (MPI-ESM1.2) for the High-Resolution Model Intercomparison Project (HighResMIP), Geoscientific Model Development, 12, 3241–3281, https://doi.org/10.5194/gmd-12-3241-2019, 2019.

Hersbach, H., Bell, B., Berrisford, P., Hirahara, S., Horányi, A., Muñoz-Sabater, J., Nicolas, J., Peubey, C., Radu, R., Schepers, D., Simmons, A., Soci, C., Abdalla, S., Abellan, X., Balsamo, G., Bechtold, P., Biavati, G., Bidlot, J., Bonavita, M., De Chiara, G., Dahlgren, P., Dee, D., Diamantakis, M., Dragani, R., Flemming, J., Forbes, R., Fuentes, M., Geer, A., Haimberger, L., Healy, S., Hogan, R. J., Hólm, E., Janisková, M., Keeley, S., Laloyaux, P., Lopez, P., Lupu, C., Radnoti, G., De Rosnay, P., Rozum, I., Vamborg, F., Villaume, S., and Thépaut, J.-N.: The ERA5 Global Reanalysis, Quarterly Journal of the Royal Meteorological Society, 146, 1999–2049, https://doi.org/10.1002/qj.3803, 2020.

IPCC: Climate Change 2021: The Physical Science Basis. Contribution of Working Group I to the Sixth Assessment Report of the Intergovernmental Panel on Climate Change, Tech. rep., IPCC, 2021.

Karger, D. N., Lange, S., Hari, C., Reyer, C. P. O., Conrad, O., Zimmermann, N. E., and Frieler, K.: CHELSA-W5E5: Daily 1 Km Meteorological Forcing Data for Climate Impact Studies, Earth System Science Data, 15, 2445–2464, https://doi.org/10.5194/essd-15-2445-2023, 2023.

Katragkou, E., Sobolowski, S. P., Teichmann, C., Solmon, F., Pavlidis, V., Rechid, D., Hoffmann, P., Fernandez, J., Nikulin, G., and Jacob, D.: Delivering an Improved Framework for the New Generation of CMIP6-Driven EURO-CORDEX Regional Climate Simulations, Bulletin of the American Meteorological Society, 105, E962–E974, https://doi.org/10.1175/BAMS-D-23-0131.1, 2024.

Kendon, E. J., Prein, A. F., Senior, C. A., and Stirling, A.: Challenges and Outlook for Convection-Permitting Climate Modelling, Philosophical Transactions of the Royal Society A: Mathematical, Physical and Engineering Sciences, 379, 20190547, https://doi.org/10.1098/rsta.2019.0547, 2021.

Lange, S.: Trend-Preserving Bias Adjustment and Statistical Downscaling with ISIMIP3BASD (v1.0), Geoscientific Model Development, 12, 3055–3070, https://doi.org/10.5194/gmd-12-3055-2019, 2019.

Lee, W.-L., Wang, Y.-C., Shiu, C.-J., Tsai, I.-c., Tu, C.-Y., Lan, Y.-Y., Chen, J.-P., Pan, H.-L., and Hsu, H.-H.: Taiwan Earth System Model Version 1: Description and Evaluation of Mean State, Geoscientific Model Development, 13, 3887–3904, https://doi.org/10.5194/gmd-13-3887-2020, 2020.

Maraun, D.: Bias Correction, Quantile Mapping, and Downscaling: Revisiting the Inflation Issue, Journal of Climate, 26, 2137–2143, https://doi.org/10.1175/JCLI-D-12-00821.1, 2013.

Maraun, D.: Bias Correcting Climate Change Simulations - a Critical Review, Current Climate Change Reports, 2, 211–220, https://doi.org/10.1007/s40641-016-0050-x, 2016.

Mauritsen, T., Bader, J., Becker, T., Behrens, J., Bittner, M., Brokopf, R., Brovkin, V., Claussen, M., Crueger, T., Esch, M., Fast, I., Fiedler, S., Fläschner, D., Gayler, V., Giorgetta, M., Goll, D. S., Haak, H., Hagemann, S., Hedemann, C., Hohenegger, C., Ilyina, T., Jahns, T., Jimenéz-de-la Cuesta, D., Jungclaus, J., Kleinen, T., Kloster, S., Kracher, D., Kinne, S., Kleberg, D., Lasslop, G., Kornblueh, L., Marotzke, J., Matei, D., Meraner, K., Mikolajewicz, U., Modali, K., Möbis, B., Müller, W. A., Nabel, J. E. M. S., Nam, C. C. W., Notz, D., Nyawira, S.-S., Paulsen, H., Peters, K., Pincus, R., Pohlmann, H., Pongratz, J., Popp, M., Raddatz, T. J., Rast, S., Redler, R., Reick, C. H., Rohrschneider, T., Schemann, V., Schmidt, H., Schnur, R., Schulzweida, U., Six, K. D., Stein, L., Stemmler, I., Stevens, B., Von Storch, J.-S., Tian, F., Voigt, A., Vrese, P., Wieners, K.-H., Wilkenskjeld, S., Winkler, A., and Roeckner, E.: Developments in the MPI-M Earth

https://doi.org/10.5194/egusphere-2025-2214
Preprint. Discussion started: 11 July 2025

System Model Version 1.2 (MPI-ESM1.2) and Its Response to Increasing CO_2, Journal of Advances in Modeling Earth Systems, 11, 998–1038, https://doi.org/10.1029/2018MS001400, 2019.

Perkins, S. E., Pitman, A. J., Holbrook, N. J., and McAneney, J.: Evaluation of the AR4 Climate Models' Simulated Daily Maximum Temperature, Minimum Temperature, and Precipitation over Australia Using Probability Density Functions, Journal of Climate, 20, 4356–4376, https://doi.org/10.1175/JCLI4253.1, 2007.

Prein, A. F., Langhans, W., Fosser, G., Ferrone, A., Ban, N., Goergen, K., Keller, M., Tölle, M., Gutjahr, O., Feser, F., Brisson, E., Kollet, S., Schmidli, J., Van Lipzig, N. P. M., and Leung, R.: A Review on Regional Convection-permitting Climate Modeling: Demonstrations, Prospects, and Challenges, Reviews of Geophysics, 53, 323–361, https://doi.org/10.1002/2014RG000475, 2015.

Saeed, S., Brisson, E., Demuzere, M., Tabari, H., Willems, P., and Van Lipzig, N. P. M.: Multidecadal Convection Permitting Climate Simulations over Belgium: Sensitivity of Future Precipitation Extremes, Atmospheric Science Letters, 18, 29–36, https://doi.org/10.1002/asl.720, 2017.

Swart, N. C., Cole, J. N. S., Kharin, V. V., Lazare, M., Scinocca, J. F., Gillett, N. P., Anstey, J., Arora, V., Christian, J. R., Hanna, S., Jiao, Y., Lee, W. G., Majaess, F., Saenko, O. A., Seiler, C., Seinen, C., Shao, A., Sigmond, M., Solheim, L., Von Salzen, K., Yang, D., and Winter, B.: The Canadian Earth System Model Version 5 (CanESM5.0.3), Geoscientific Model Development, 12, 4823–4873, https://doi.org/10.5194/gmd-12-4823-2019, 2019.

Switanek, M., Maraun, D., and Bevacqua, E.: Stochastic Downscaling of Gridded Precipitation to Spatially Coherent Subgrid Precipitation Fields Using a Transformed Gaussian Model, International Journal of Climatology, 42, 6126–6147, https://doi.org/10.1002/joc.7581, 2022.

Tatebe, H., Ogura, T., Nitta, T., Komuro, Y., Ogochi, K., Takemura, T., Sudo, K., Sekiguchi, M., Abe, M., Saito, F., Chikira, M., Watanabe, S., Mori, M., Hirota, N., Kawatani, Y., Mochizuki, T., Yoshimura, K., Takata, K., O'ishi, R., Yamazaki, D., Suzuki, T., Kurogi, M., Kataoka, T., Watanabe, M., and Kimoto, M.: Description and Basic Evaluation of Simulated Mean State, Internal Variability, and Climate Sensitivity in MIROC6, Geoscientific Model Development, 12, 2727–2765, https://doi.org/10.5194/gmd-12-2727-2019, 2019.

Termonia, P., Van Schaeybroeck, B., De Cruz, L., De Troch, R., Caluwaerts, S., Giot, O., Hamdi, R., Vannitsem, S., Duchêne, F., Willems, P., Tabari, H., Van Uytven, E., Hosseinzadehtalaei, P., Van Lipzig, N., Wouters, H., Vanden Broucke, S., Van Ypersele, J.-P., Marbaix, P., Villanueva-Birriel, C., Fettweis, X., Wyard, C., Scholzen, C., Doutreloup, S., De Ridder, K., Gobin, A., Lauwaet, D., Stavrakou, T., Bauwens, M., Müller, J.-F., Luyten, P., Ponsar, S., Van Den Eynde, D., and Pottiaux, E.: The CORDEX.Be Initiative as a Foundation for Climate Services in Belgium, Climate Services, 11, 49–61, https://doi.org/10.1016/j.cliser.2018.05.001, 2018.

Van De Velde, J., Demuzere, M., De Baets, B., and Verhoest, N.: Future Multivariate Weather Generation by Combining Bartlett-Lewis and Vine Copula Models, Hydrological Sciences Journal, 68, 1–15, https://doi.org/10.1080/02626667.2022.2144322, 2023.

Vanden Broucke, S., Wouters, H., Demuzere, M., and Van Lipzig, N. P. M.: The Influence of Convection-Permitting Regional Climate Modeling on Future Projections of Extreme Precipitation: Dependency on Topography and Timescale, Climate Dynamics, 52, 5303–5324, https://doi.org/10.1007/s00382-018-4454-2, 2019.

Volodin, E. M., Mortikov, E. V., Kostrykin, S. V., Galin, V. Ya., Lykossov, V. N., Gritsun, A. S., Diansky, N. A., Gusev, A. V., and Iakovlev, N. G.: Simulation of the Present-Day Climate with the Climate Model INMCM5, Climate Dynamics, 49, 3715–3734, https://doi.org/10.1007/s00382-017-3539-7, 2017.

Volodin, E. M., Mortikov, E. V., Kostrykin, S. V., Galin, V. Y., Lykossov, V. N., Gritsun, A. S., Diansky, N. A., Gusev, A. V., Iakovlev, N. G., Shestakova, A. A., and Emelina, S. V.: Simulation of the Modern Climate Using the INM-CM48 Climate Model, Russian Journal of Numerical Analysis and Mathematical Modelling, 33, 367–374, https://doi.org/10.1515/rnam-2018-0032, 2018.

https://doi.org/10.5194/egusphere-2025-2214
Preprint. Discussion started: 11 July 2025

Volosciuk, C., Maraun, D., Vrac, M., and Widmann, M.: A Combined Statistical Bias Correction and Stochastic Downscaling Method for Precipitation, Hydrology and Earth System Sciences, 21, 1693–1719, https://doi.org/10.5194/hess-21-1693-2017, 2017.

Wouters, H.: EXSoDOS: Downscaling of Changing Weather Extremes for Climate Projections: Code and Input Data for Demonstration, Zenodo, https://doi.org/10.5281/zenodo.15387101, 2025.

Wouters, H., Demuzere, M., Blahak, U., Fortuniak, K., Maiheu, B., Camps, J., Tielemans, D., and Van Lipzig, N. P. M.: The Efficient Urban Canopy Dependency Parametrization (SURY) v1.0 Foratmospheric Modelling: Description and Application with the COSMO-CLM Modelfor a Belgian Summer, Geoscientific Model Development, 9, 3027–3054, https://doi.org/10.5194/gmd-9-3027-2016, 2016.

Wouters, H., De Ridder, K., Poelmans, L., Willems, P., Brouwers, J., Hosseinzadehtalaei, P., Tabari, H., Vanden Broucke, S., van Lipzig, N. P. M., and Demuzere, M.: Heat Stress Increase under Climate Change Twice as Large in Cities as in Rural Areas: A Study for a Densely Populated Midlatitude Maritime Region, Geophysical Research Letters, 44, 8997–9007, https://doi.org/10.1002/2017GL074889, 2017.

Wouters, H., Keune, J., Petrova, I. Y., Van Heerwaarden, C. C., Teuling, A. J., Pal, J. S., Vilà-Guerau De Arellano, J., and Miralles, D. G.: Soil Drought Can Mitigate Deadly Heat Stress Thanks to a Reduction of Air Humidity, Science Advances, 8, eabe6653, https://doi.org/10.1126/sciadv.abe6653, 2022.

Yukimoto, S., Kawai, H., Koshiro, T., Oshima, N., Yoshida, K., Urakawa, S., Tsujino, H., Deushi, M., Tanaka, T., Hosaka, M., Yabu, S., Yoshimura, H., Shindo, E., Mizuta, R., Obata, A., Adachi, Y., and Ishii, M.: The Meteorological Research Institute Earth System Model Version 2.0, MRI-ESM2.0: Description and Basic Evaluation of the Physical Component, Journal of the Meteorological Society of Japan. Ser. II, 97, 931–965, https://doi.org/10.2151/jmsj.2019-051, 2019.